Evaluation of Nonlinear Control Performance of Air Handling Units under Variable Operation Conditions using Root Distribution Approach

Zufen Wang[1], Choon Yik Tang[2], Rodney Hurt[3], Li Song[3], Gang Wang[1]

1. Department of Civil, Architectural and Environmental Engineering, University of Miami, Coral Gables, FL 33146, USA
2. School of Electrical and Computer Engineering, University of Oklahoma, Norman, OK 73019, USA
3. School of Aerospace and Mechanical Engineering, University of Oklahoma, Norman, OK 73019, USA

Abstract

The control systems at Air handling units (AHUs) have nonlinear nature, resulting potentially in sluggish, aggressive, or oscillatory responses under variable operation conditions. This paper is to develop an approach for evaluating the nonlinear control performance of AHUs under variable operation conditions and for identifying the impact of varying multiple operation parameters which guides controller design. To do so, an *operation parameter-based root distribution* technique, intended to sketch the paths traced by closed-loop poles as multiple operation parameters are varied, is first introduced. The technique—which may be viewed as an extension of conventional, single-variable root locus—is then applied to a fan speed control system that includes a motor with a variable frequency drive and a supply fan with an air duct under variable fan speed and duct static pressure. Using the technique, the system's stability region is graphically identified. The system is also found to be aggressive and gradually lose its stability as the fan speed decreases and the duct static pressure increases, which is validated by the field tests. The root distribution approach is an effective tool to

evaluate the performance of any nonlinear control systems at AHUs with multiple variable operation parameters without requiring time-domain simulations.

1. Introduction

Heating, ventilation, and air-conditioning (HVAC) systems are an indispensable part of commercial buildings, ensuring their thermal comfort and indoor environment quality. Such systems account for almost 50% of the energy consumed in commercial buildings and around 10–20% of the total energy consumption in developed countries (Pérez Lombard, Ortiz, and Pout 2008). Moreover, the energy waste of HVAC systems is estimated to reach 25% to 77% due to improper design and operation of their control systems (Barwig et al. 2002).

1.1 Control issues at air handling units

Air handling units (AHUs) are intended to ensure space thermal comfort and indoor air quality in large commercial buildings through several control systems, including the supply fan speed control, chilled-water cooling coil valve control, and outdoor air damper control. The fan speed control system consists of the supply fan driven by a motor with a variable frequency drive (VFD) and an air duct as well as a duct static pressure sensor. The supply fan speed is modulated to maintain a duct static pressure setpoint. The cooling coil valve control system consists of a chilled-water cooling coil, a control valve with an actuator, and a supply air temperature sensor. The valve position is modulated to maintain the supply air temperature setpoint (Underwood 2002). The outdoor air damper control system consists of a set of control dampers, including outdoor air, recirculation air and relief air dampers, along with an outdoor airflow sensor and a supply air temperature sensor shared with the cooling coil valve control.

The damper positions are modulated to maintain a minimum outdoor airflow rate setpoint in the minimum outdoor air mode and a supply air temperaure setpoint in the economizer mode (Nassif 2010).

Generally, the components in the three control systems—such as the air duct, cooling coil, control valve and air dampers— are all nonlinear in nature, i.e., the component gain (the ratio of its control output or response change to its control input change) and the component time constant (the time for its step response to reach 63% of its final value) will vary nonlinearly with operation conditions, such as the duct static pressure and fan speed or airflow rate in the fan speed control system. In this paper, the component gain and time constant are referred to as *control parameters* while the parameters representing the operation conditions, such as the duct static pressure, fan speed, and airflow rate, are referred to as *operation parameters*. Extensive research has shown that the control parameters at AHUs can be highly dependent on the operation parameters.

The experiments conducted by Mei and Levermore (Mei and Levermore 2002) show that the response of fan head has variable time constant from 4s to 20s corresponding to duct static pressure from 650 Pa to 710 Pa when the motor supply voltage experiences a step change. The study conducted by Lachi, El Wakil et al. (Lachi, El Wakil, and Padet 1997) reveals that the cooling/heating coil time constant can be impacted by the mixing air temperature and supply airflow rate. Their experimental results verify that the time constant indeed decreases with the decrease in supply airflow rate. The nonlinearity characterization conducted by Singhal and Salsbury (Singhal and Salsbury 2007) shows that the plant of the heating/cooling coil and valve has a larger gain at lower supply airflow rate conditions. In addition, it is also pointed out that the plant nonlinearity can be impacted by the valve

position and the entering air and water temperature. The performance of the outdoor air damper control system investigated by Wang, Song et al. (Wang, Song, and Phalak 2015) found that the ratio of the maximum total system gain (the derivative of the controlled variable with respect to the control input) to the minimum total system gain can reach from 1 to 2.1 as the outdoor airflow ratio varies from 0.05 to 1.

With the increasing deployment of occupancy sensors in commercial buildings, information generated by such sensors can be used to dynamically reset the outdoor airflow and terminal box minimum airflow setpoints to conserve energy. However, the resets can significantly and frequently affect the dynamics of the fan speed, cooling coil valve position, and outdoor air damper position at AHUs. On the other hand, the duct static pressure, supply air temperature and minimum outdoor airflow setpoint reset will also change the operation conditions of the control systems.

Because the control parameters at AHUs are highly dependent on the operation parameters, the frequently variable operation conditions make the control system design a non-trivial problem. Traditionally, the three control systems are each designed to be a single-loop feedback control system with a Proportional-Integral-Derivative (PID) controller, whose gains are fixed regardless of operation conditions in building automation systems. With such a controller, the system can become sluggish or oscillatory when its component gains deviate significantly from the values that were used to tune the controller (Singhal and Salsbury 2007). Worse yet, the system can experience instability when it operates at low-load conditions if the controller was tuned for high-load conditions (Underwood 2002; Moradi, Saffar-Avval, and Bakhtiari-Nejad 2011; Price, Liang, and Rasmussen 2015). As a result,

unwanted oscillations have often been observed at AHUs. Indeed, in a test conducted on ten AHUs (Chintala et al. 2015) , oscillations were observed in 22% of the supply fans for 6%–26% of their operating time and in 70% of the cooling coil valves for 6%–78% of their operating time. As the oscillations can result in higher energy consumption, thermal discomfort sacrifice and equipment wear, it is essential to understand the impact of variable operation parameters on the nonlinear control performance so that controller design and tuning can be more effectively carried out. Generally, to achieve this objective, extensive time-domain simulations and experimental tests need to be conducted under various operation conditions (Price 2018; Adebayo, Aborisade, and Yinka 2020; Almabrok, Psarakis, and Dounis 2018), which is time and cost consuming and sometimes even infeasible. Therefore, to avoid the laborious work, a more efficient approach is expected.

1.2 Merit and limitations of root locus technique

For a linear time-invariant (LTI) feedback control system, the Laplace transform of its output can be expressed as the product of the Laplace transform of its input, which can be either a reference input or a disturbance input, and its closed-loop transfer function. The closed-loop poles, defined as the roots of the characteristic equation of the closed-loop transfer function, can give valuable insight into the control performance, such as whether the system is stable, oscillatory, sluggish, and aggressive.

Because closed-loop poles are important, methods that shed light on their locations have been developed, including the root locus technique by Evans (Evans 1948). With this technique, one could graphically visualize how the closed-loop poles move around in the complex plane, tracing out a set of paths called *root loci*, as a control parameter—typically the gain of a P controller (K_p)—is varied. The

technique allows one to implicitly compute the closed-loop poles which are roots of the characteristic equation:

$$1 + K_p G(s)H(s) = 0 \quad (1)$$

where $G(s)$ is the forward path transfer function, $H(s)$ is the feedback path transfer function, and $K_p G(s)H(s)$ is the open-loop transfer function. The root locus of a closed-loop system gives qualitative information about its behavior as K_p is varied without requiring extensive time-domain simulations. For example, if one of the root loci breaks into the right-half plane (RHP), that means the system is unstable whenever K_p exceeds a critical value (that can be determined using the Routh-Hurwitz criterion). Furthermore, a technique, the generalized root locus, can be used to analyze system stability and transient response as one of the parameters other than the K_p is varied, so that the impact of the studied parameter can be understood (Nise 2019).

Recognizing its usefulness, some studies have extended the root locus technique to identify the impact of the system operation parameters to its control performance. Flower and Hodge (Flower and Hodge 2004) applied the root locus technique to a power distribution system for assessing the effect of varying capacitance or load resistance on the power system stability and transient response. Al-Khayat et al (Al-Khayat et al. 2022) applied the root locus technique to study the impact of the pressure, flow velocity, conduit diameter, and the liquid's density on the water hammer phenomenon separately. They linked the varying operation parameter to K_p in Equation (1) to sketch the root loci. However, in their studies, the remaining parameters had to be fixed while only the studied parameter was varied. It means

that, by using the conventional root locus technique, only one varying parameter can be studied at a time while the integral impact of the multiple operation parameters cannot be obtained.

Similarly, this paper attempts to apply the idea of root locus to the control systems at AHUs to look at the impact of operation parameters that HVAC engineers are often more interested in. For the attempt to succeed, however, a major hurdle must be overcome: Conventional root locus is applicable only to LTI control systems whose control parameters vary one at a time. It is not applicable to the control systems at AHUs, because their component gains and time constants can vary simultaneously and nonlinearly as one or multiple operation parameters vary.

Motivated by the above considerations, this paper aims at developing an approach for evaluating the performance of nonlinear control systems at AHUs under variable operation conditions and for identifying the impact of varying multiple operation parameters which guides controller design. To achieve the aim, this paper first introduces an operation parameter-based root distribution technique that extends conventional root locus to nonlinear control systems. The paper then demonstrates the technique by applying it to a fan speed control system, whose control performance under variable operation conditions, represented by the duct static pressure and fan speed, is evaluated. Finally, the paper validates the reliability of the root distribution through field tests.

2. Development of operation parameter-based root distribution

In this section, a general single-loop feedback control system and the conventional root locus technique will first be introduced. Based on the latter, a novel operation parameter-based root distribution technique will be developed.

2.1 Control configuration and closed-loop transfer function

Consider a general single-loop feedback control system consisting of a controller, an actuator, a plant, and a sensor. The forward path includes the plant, actuator and controller while the feedback path includes the sensor. As shown in Fig. 1, the control system is intended to make the controlled variable (C) track the reference input (R) irrespective of the disturbance inputs (D_1 and D_2), which act at different locations of the plant.

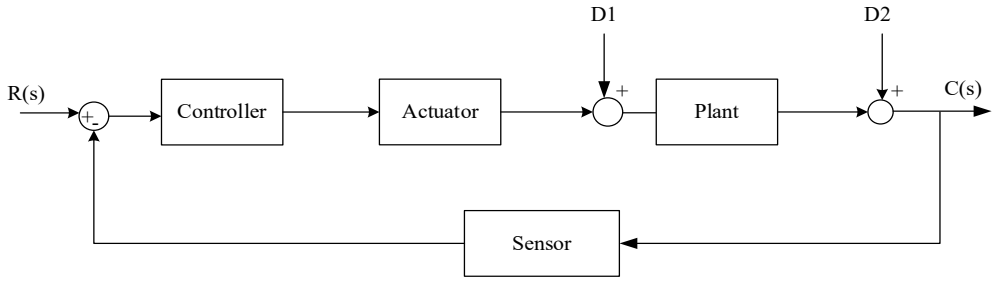

Fig. 1 Block diagram of a general single-loop feedback control system.

The block diagram in Fig. 1 can be used to model the three control systems at an AHU (fan speed, cooling coil valve, and outdoor air damper) by associating the actuator, plant, and sensor blocks with the components of the three control systems listed in Table 1.

Table 1: Components of the control systems at an AHU

Components	Actuator	Plant	Sensor
Fan speed control	Fan	Air duct	Static pressure differential sensor
Cooling coil valve control	Control valve	Cooling coil	Temperature sensor
Outdoor air damper control	Control dampers	Mixing chamber	Airflow or temperature sensor

Assume that the control system in Fig. 1 is LTI and the actuator, plant, and sensor components (ct) are each a first-order model with the constant gain (K_{ct}) and time constant (τ_{ct}), as shown in Eq. (2).

Also assume that the PI controller (C) with the P gain (K_P) and I gain (K_I) has the form shown in Eq. (3).

$$G_{ct}(s) = \frac{K_{ct}}{\tau_{ct}s+1} \tag{2}$$

$$G_C(s) = K_P\left(1 + \frac{K_I}{s}\right) \tag{3}$$

Then, the closed-loop transfer function of the control system with the reference input can be expressed as

$$G(s) = \frac{C(s)}{R(s)} = \frac{G_C(s)G_{ac}(s)G_{pt}(s)}{1+G_C(s)G_{ac}(s)G_{pt}(s)G_{sr}(s)} = \frac{K_P\left(1+\frac{K_I}{s}\right)\left(\frac{K_{ac}}{\tau_{ac}s+1}\right)\left(\frac{K_{pt}}{\tau_{pt}s+1}\right)}{1+K_P\left(1+\frac{K_I}{s}\right)\left(\frac{K_{ac}}{\tau_{ac}s+1}\right)\left(\frac{K_{pt}}{\tau_{pt}s+1}\right)\left(\frac{K_{sr}}{\tau_{sr}s+1}\right)} \tag{4}$$

where G_{ac}, G_{ac}, G_{ac} are the transfer functions of the actuator, plant and sensor, respectively, K_{ac}, K_{pt}, K_{sr} are the gains of the actuator, plant, and sensor, respectively, and τ_{ac}, τ_{pt}, τ_{sr} are their time constants. The denominator in Eq. (4) is the right-hand side of the characteristic equation, defined by Eq. (1). The component gains and time constants as well as the controller P gain and I gain are all referred to as the control parameters as defined in this paper. Because the PI controllers are generally designed to be fixed regardless of operation conditions for the control systems at AHUs while the component gains and time constants may vary with the operation conditions, the P gain and I gain will be fixed while the component gains and times will be mainly studied in this paper.

2.2 Conventional root locus technique

The root locus technique can be used to analyze the control system performance when a parameter of interest is varied, such as component gain, time constant, or controller gain. To do so, however, the characteristic equation of the closed-loop transfer function in Eq. (4) should first be converted into the form of Eq. (1), with the interested parameter to be varied. The root locus (i.e., paths of the closed-loop

poles) can then be hand-sketched using a standard procedure (Nise 2019) or drawn using the *rlocus* command in MATLAB. The control system stability and transient response under variable K_P can subsequently be evaluated by examining the root locus on the s-plane.

Mulligan (Mulligan 1949) first investigated the feasibility of approximating the performance of a linear control system with a step input using only dominant poles. Since then, plenty of studies have been conducted which show that a pole may be considered dominant if its (negative) real part is at least 3 to 5 times smaller than the (negative) real part of all other poles and if there are no zeros nearby (Dincel and Söylemez 2016; Wang et al. 2009). In the case where the root locus shows a pair of dominant, complex conjugate poles $-\sigma_d \pm j\omega_d$ —implying that the control system may be approximated by a second-order, underdamped system—the settling time, peak time, and percent overshoot can be calculated as follows (Nise 2019):

$$t_{settling} = \frac{4}{\sigma_d} \tag{5a}$$

$$t_{peak} = \frac{\pi}{\omega_d} \tag{5b}$$

$$\%OS = e^{-\left(\frac{\pi}{\tan\theta}\right)} \times 100 \tag{5c}$$

where $\theta = \tan^{-1}\frac{\omega_d}{\sigma_d}$ is the angle between the pole and the negative real axis. Eqs. (5) reveal that the settling time is inversely proportional to the real part (σ_d), the peak time is inversely proportional to the imaginary part (ω_d), and the percent overshoot increases with the angle (θ). Note that Eqs. (5) are no longer valid if the poles move into the RHP, making the system unstable, or break into the real axis, making it overdamped.

2.3 Operation parameter-based root distribution

As mentioned in the Introduction, conventional root locus technique is applicable only to control systems that are linear, whose control parameters vary one, mostly the P gain of the controller, at a time and whose characteristic equation can be expressed by Eq. (1). The control systems at AHUs, unfortunately, do not satisfy these conditions because their component gains and time constants in Eq. (4) may vary simultaneously and nonlinearly as multiple operation parameters vary, due to which the characteristic equation cannot be cast into the form of Eq. (1). Consequently, the standard procedure for sketching root locus cannot be used. Nevertheless, the idea of using root locus to analyze control system performance is still an attractive one. Also attractive is the fact that the control parameters are functions of the operation parameters, thus providing a direct link between the ultimate control performance and the physical operation parameters. To enable the idea of root locus and benefit from such a direct link, the concept of operation parameter-based root distribution and a procedure for sketching it are introduced next.

Recall that the control system in Fig. 1 has three first-order components and a PI controller in the form of Eqs. (2) and (3). For a specific system, such as the fan speed control system, it has three first-order components (a motor with a VFD, a supply fan with an air duct, and a duct static pressure sensor) and a PI controller with fixed gains, which together produce four closed-loop poles.

In fact, three operation parameters, including the duct static pressure, fan speed and fan airflow rate, are involved in the fan speed control system. However, only two of them are independent. Since the duct static pressure and fan speed are measurable at AHUs, they are selected as the independent

operation parameters. The approaches with one varying operation parameter and with two varying operation parameters are discussed, respectively.

First it is assumed that the fan speed control system has one varying operation parameter, using the variable fan speed in the explanation, which varies at a number (Num) of different values and generates a same number (Num) of operation conditions. Since the closed-loop poles are varied with only one varying operation parameter, the paths of the closed-loop poles corresponding to Num values of the fan speed can still be sketched in the s-plane and be applied to evaluate the control system stability and transient response, which is the same as the root locus technique except that the sketching procedure is different, stated as follows:

Step 1: Obtain the three component gains and time constants as the function of the fan speed by linearizing the nonlinear differential equations of the system model or by regressing through open-loop tests with a step response around an operation condition.

Step 2: Create the closed-loop transfer function by using the three component gains and time constants at Num values of the fan speed, which generate Num operation conditions.

Step 3: Compute the closed-loop poles of the closed-loop transfer function by using the *pole* command in MATLAB corresponding to the Num operation conditions.

Step 4: Obtain the operation parameter-based root distribution by drawing the closed-loop poles from Step 3 by adding the corresponding fan speed on the s-plane as the third dimension (Z-axis).

Second, if two operation parameters, the fan speed and duct static pressure, are to be varied, the component gains and time constants at Step 1 would be derived as the function of the fan speed and

duct static pressure, the closed-loop transfer function at Step 2 and the closed-loop poles at Step 3 would be obtained at Num_1 values of the first parameter (the fan speed) and Num_2 values of the second parameter (the duct static pressure), resulting in $Num = Num_1 \cdot Num_2$ various operation conditions using the procedure as the same as one with a single varying operation parameter. On the other hand, the operation parameter-based root distribution would have to be drawn as a four-dimensional figure with the real axis, imaginary axis and two operation parameters axes. In this case, the real and imaginary parts of this pole can be presented separately to convert it to two three-dimensional figures with the real part and imaginary part as the Z axis respectively and two operation parameters as the X and Y axes for a clearer view.

Afterward, the sketched root distribution under variable operation parameters is applied to evaluate the control system performance as the same as using the conventional root locus approach.

It has to be noted that the number of the operation conditions to be generated in Step 2 should consider the sensitivity and monotonicity of the component gains and time constants to the operation parameter's change. Especially, if the component gains and time constants are sensitive to the operation parameter's change and its impact is nonmonotonic, more operation conditions should be generated to guarantee that the nonlinear characteristics can be caught.

Even though the primary purpose of the developed root distribution approach is to evaluate the control performance of nonlinear control systems with multiple variable operation parameters, it can also be applied to the linear control systems with one varying control parameter. The comprehensive comparison between the conventional root locus and proposed root distribution is shown in Table 2.

Table 2: Comparison of conventional root locus and proposed root distribution

		Root locus	Root distribution	
Shared mechanism		Closed-loop poles		
Difference	Number of varying parameters	Only one	One	Two (or more)
	Studied parameter(s) in general	Control parameters, such as gain (K_p)	Operation parameters (μ_1, μ_2), such as fan speed and duct static pressure, in addition to control parameters, such as gain (K_p)	
	Applicable system type	Linear	Linear or nonlinear	
	Characteristic equation format	$\mathcal{T}(K_p) = 1 + K_p G(s)H(s)$	$\mathcal{T}(\mu_1)$ or $\mathcal{T}(K_p)$ in any format	$\mathcal{T}(\mu_1, \mu_2)$ in any format
	Sketching method in MATLAB	Only one *rlocus* command	Repeated *pole* command at each operation condition	
	Visualization	The paths of poles in a complex plane with the real part as X axis, the imaginary part Y axis, and some typical values of the studied parameter marked.	The poles in a three-dimensional space with the real part as X axis, the imaginary part Y axis and the studied parameter as Z axis.	The real and imaginary parts of the poles in two separate three-dimensional spaces with the two studied parameters as X and Y axes and the real or imaginary part as Z axis.

2.4 General operation parameter-based root distribution

For a general nonlinear control system, the number of impacting operation parameter may be more than 2. For instance, in the cooling coil valve control system, the operation parameters include the chilled-water supply temperature and chilled-water loop pressure differential in addition to the supply airflow rate and mixing air temperature. Moreover, the control system can have more components besides the actuator, plant, and sensor and the controller can be a PID control instead of a PI control. Thus, a general operation parameter-based root distribution approach needs to be developed.

It is assumed that it has n first-order components and a fixed lth-order controller, which together produce $k = n + l$ closed-loop poles. Moreover, it is assumed to have m operation parameters which, when viewed as a vector, can have Num different values corresponding to Num operation conditions. With this setup, the procedure for sketching its operation parameter-based root distribution is stated as follows (see also Fig. 2):

Step 1: Obtain a possibly nonlinear, physical model for the closed-loop system and identify the m operation parameters $(\mu_1, \mu_2, \dots, \mu_m)$, including the one to be varied and studied (μ_{sd}).

Step 2: Derive the n component gains $(K_1, K_2, \dots, K_n)$ and n time constants $(\tau_1, \tau_2, \dots, \tau_n)$ as functions of the m operation parameters $(\mu_1, \mu_2, \dots, \mu_m)$ by linearizing the physical model from Step 1 around operation condition $(\mu_1, \mu_2, \dots, \mu_m)$.

Step 3: Determine a range of Num values over which the operation parameter to be studied (μ_{sd}) varies, while keeping the remaining $m - 1$ operation parameters fixed, to generate Num operation conditions. For $i = 1,2, \dots, Num$, use the ith operation condition $(\mu_{1,i}, \mu_{2,i}, \dots, \mu_{m,i})$ and the functions from Step 2 to compute the n component gains $(K_{1,i}, K_{2,i}, \dots, K_{n,i})$ and n time constants $(\tau_{1,i}, \tau_{2,i}, \dots, \tau_{n,i})$ as well as the closed-loop transfer function $T_i(s)$.

Step 4: For $i = 1,2, \dots, Num$, compute the k closed-loop poles $(Po_{1,i}, Po_{2,i}, \dots, Po_{k,i})$ using the closed-loop transfer function $T_i(s)$ from Step 3.

Step 5: For $i = 1,2, \dots, Num$, draw the k closed-loop poles $(Po_{1,i}, Po_{2,i}, \dots, Po_{k,i})$ from Step 4 on the s-plane to obtain the operation parameter-based root distribution.

Similarly, if all the m operation parameters are to be varied, there would be $Num = Num_1 \cdot Num_2 \cdot \ldots \cdot Num_m$ operation conditions, and the root distribution would be an $(m+2)$ dimensional figure (that needs special techniques to help visualize).

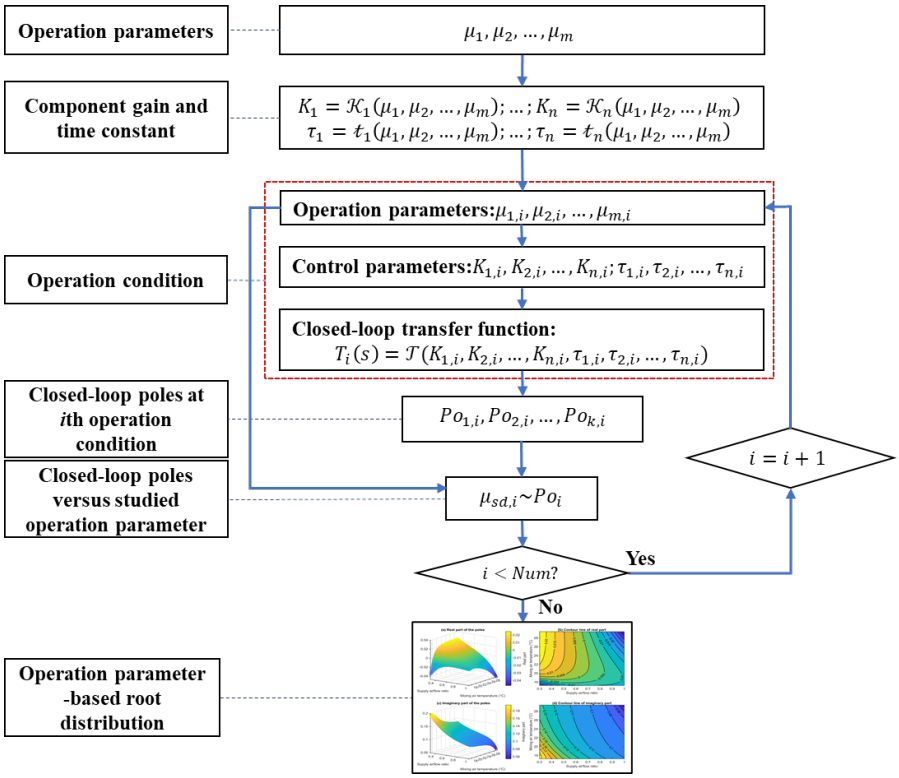

Fig. 2 Flowchart for sketching general operation parameter-based root distribution.

Since the developed root distribution approach shares the same mechanism, using the closed-loop poles, with the conventional root locus method, the evaluation results of the two approaches should be exactly the same for the linear control systems with one varying control parameter. However, only the root distribution approach can be applied to evaluate the control performance of the nonlinear control systems with multiple variable control or operation parameters.

3 Application

The fan speed control system is taken as an example to illustrate the application of the developed root distribution approach. By following the procedure developed in Section 2.3, the open-loop tests are first conducted to obtain the component gains and time constants of VFD-motor and fan-duct, which are regressed as functions of the fan speed and duct static pressure. Then, 80 operation conditions for varying fan speed and duct static pressure are generated, and the corresponding component gains and time constants as well as the transfer functions are determined. Afterwards, the closed-loop poles are computed, and the root distribution is sketched.

3.1 Fan speed control system model

The schematics of the fan speed control system at an AHU is shown as Fig. 3. The tests were conducted on a single duct AHU which serves an education building in Norman, Oklahoma. The duct static pressure sensor is located two-thirds of the way downstream of the supply air duct with four terminal boxes at the downstream and three terminal boxes at the upstream of the static pressure sensor. The fan is powered by a 3ph 208V 2.2 kW motor through a VFD, with a design fan airflow rate of 1,180 L/s and a design fan head of 547 Pa. During the tests, the VFD frequency command (CO) and fan speed (N) are directly obtained from the VFD. The VFD analog output frequency data can accurately reflect the actual VFD output frequency with the errors less than 0.01Hz (Wang and Han 2019). And the duct static pressure (H_{sp})is measured using a duct static pressure sensor (P) with an accuracy of ±0.4% of full scale (0 to 1244 Pa). All the test data were recorded at 1 second interval.

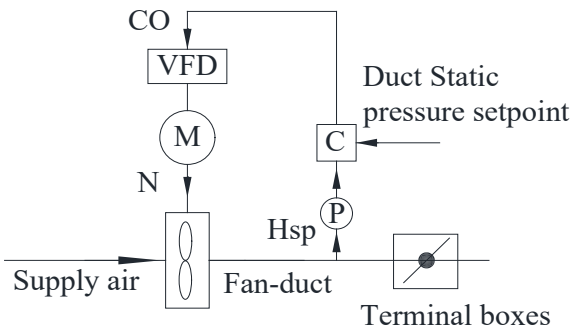

Fig. 3 Schematic of fan speed control at an AHU.

Theoretically, the component gains and time constants can be derived from the nonlinear physical model by expanding the nonlinear functions into a Taylor series around the operation condition with a small excursion of the VFD frequency command or fan speed and retaining the only linear term (Nise 2019). The VFD-motor gain (K_{Vm}) is defined as the ratio of the fan speed change to VFD frequency command change while the fan-duct gain (K_{fd}) is defined as the ratio of the duct static pressure change to fan speed change.

Considering its complexity to build the theoretical model of the components, this paper calibrates the gains and time constants of the VFD-motor and fan-duct through a set of open-loop tests. Ideally, the open-loop tests are designed with a step change of the VFD frequency command at an operation condition (the ith operation condition) and the VFD-motor gain (K_{Vm}) can be calculated based on the steady-state values of the VFD frequency command and fan speed at the ith operation condition and its corresponding condition after a step change (the $(i+1)$th operation condition), shown as Eq. (6). And the VFD-motor time constant can be obtained through the time response by measuring the time for the fan speed to reach 63% of its final value. Similarly, the fan-duct gain (K_{fd}) can be calculated based on the steady-state values of the fan speed and duct static pressure with a step change of the fan speed,

shown as Eq. (7), while the fan-duct time constant can be obtained from the time response of the duct static pressure.

$$K_{Vm,i} = \frac{N_{i+1} - N_i}{CO_{i+1} - CO_i} \tag{6}$$

$$K_{fd,i} = \frac{H_{sp,i+1} - H_{sp,i}}{N_{i+1} - N_i} \tag{7}$$

where i ($i = 1,2,3, \ldots$) refers to the ith operation condition; CO_i, N_i and $H_{sp,i}$ are the steady-state values of the VFD frequency command, fan speed and duct static pressure at the ith operation condition.

In the real operation, the duct static pressure is controlled by the fan speed, thus, the duct static pressure is correlated to the fan speed based on the damper positions of terminal boxes. Three open-loop tests were designed with different fixed damper positions and incrementally changed fan speed to create operation conditions with independent duct static pressure and fan speed. To fully open one terminal box, the minimum airflow setpoint is set to be higher than its capacity while, on the other hand, to fully close one terminal box, the maximum airflow setpoint is set to be zero. The first test was conducted with all the dampers overridden at the fully open position while the second and the third tests were conducted by fully closing three dampers of the seven terminal boxes and then five dampers of the seven terminal boxes, respectively. For each test, the VFD frequency command was overridden from 29Hz to 38Hz, 47Hz, 56Hz and 58Hz respectively by a step change of the VFD frequency command. At each operation condition, the system operated for about 8 minutes. The design of the three open-loop tests is listed in Table 3.

Table 3: Design of the three open-loop tests.

Test	Number of dampers fully closed	Number of dampers fully open	VFD frequency command
First test	0	7	A step change from 29Hz to 38Hz, 47Hz, 56Hz and 58Hz respectively with a time interval of 8 minutes
Second test	3	4	
Third test	5	2	

Fig. 4 presents the fan speed (red line), VFD frequency command (green line) and duct static pressure (blue line) when five terminal box dampers were fully closed with the step changes of the VFD frequency command.

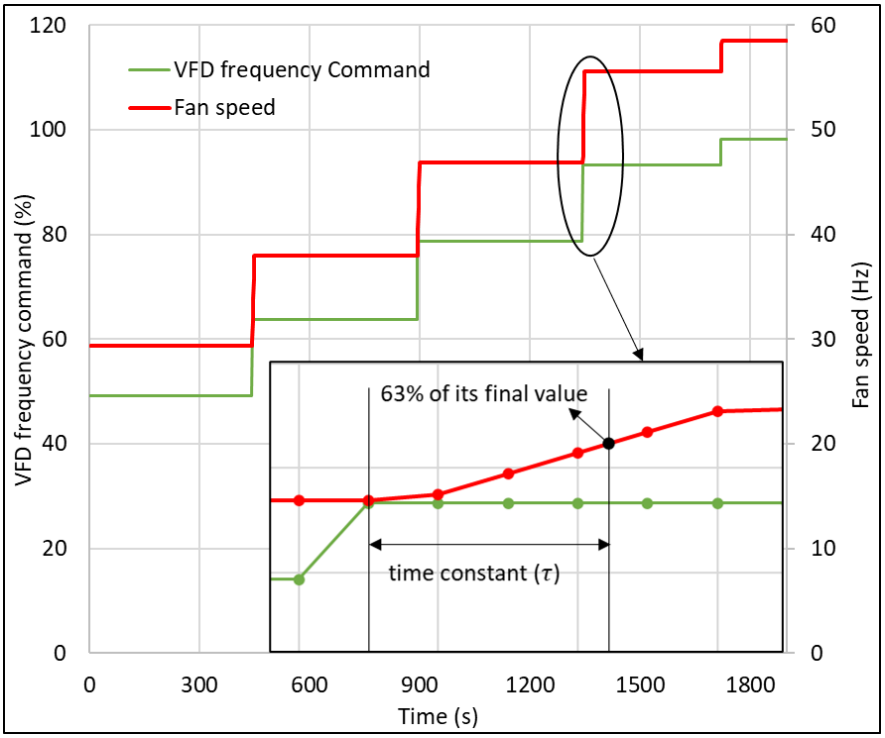

Fig. 4(a) VFD frequency command and fan speed

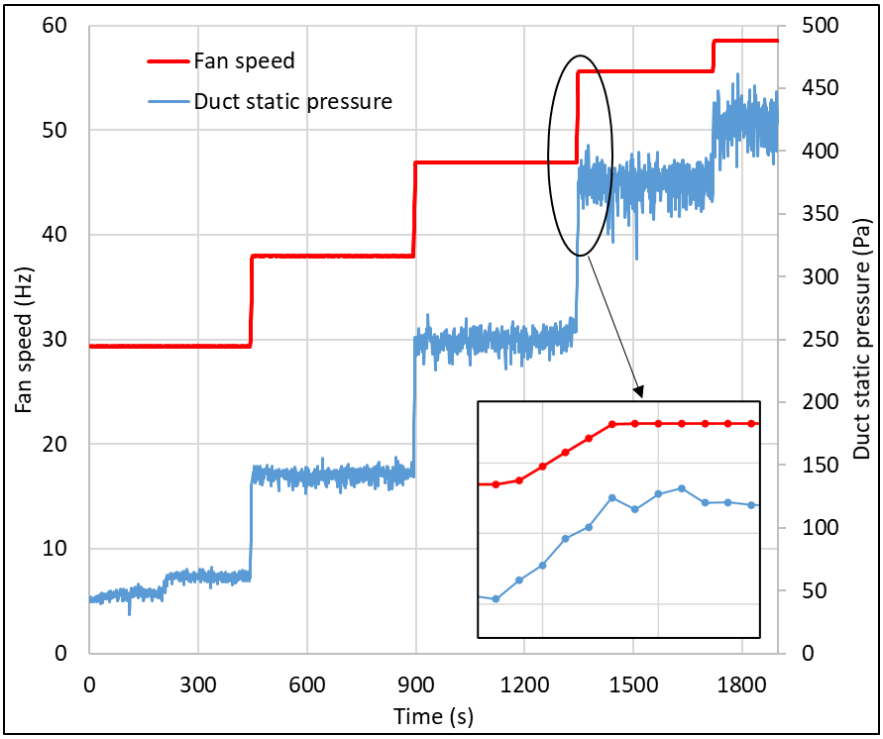

Fig. 4(b) Fan speed and duct static pressure

Fig. 4 Fan speed, VFD frequency command and duct static pressure with five dampers closed.

According to the test results in Fig. 4(a), the VFD-motor gain is calculated as a fixed value of 0.6 Hz/% based on Eq. (6), which is same as the ratio of the full range of the fan speed (60Hz) to the full range of the VFD frequency command (100%), while the VFD-motor time constant is measured to be around 3 seconds.

On the other hand, the fan-duct gain under each operation condition can be calculated based on Eq. (7). Fig. 5 shows the fan-duct gain versus duct static pressure with different fan speed groups marked by diamonds with different colors. As for the fan-duct time constant, it is observed in Fig. 4(b) that the time response of the fan-duct to the fan speed change is too fast and the time constant is less than 1 second, for which the recorded data cannot catch the specifications of its dynamic response. In this case, this paper approximates the fan-duct time constant as 0.5 second. Because the fan-duct time constant is

much smaller than the VFD-motor time constant, the uncertainty of the approximation will not have considerable impact.

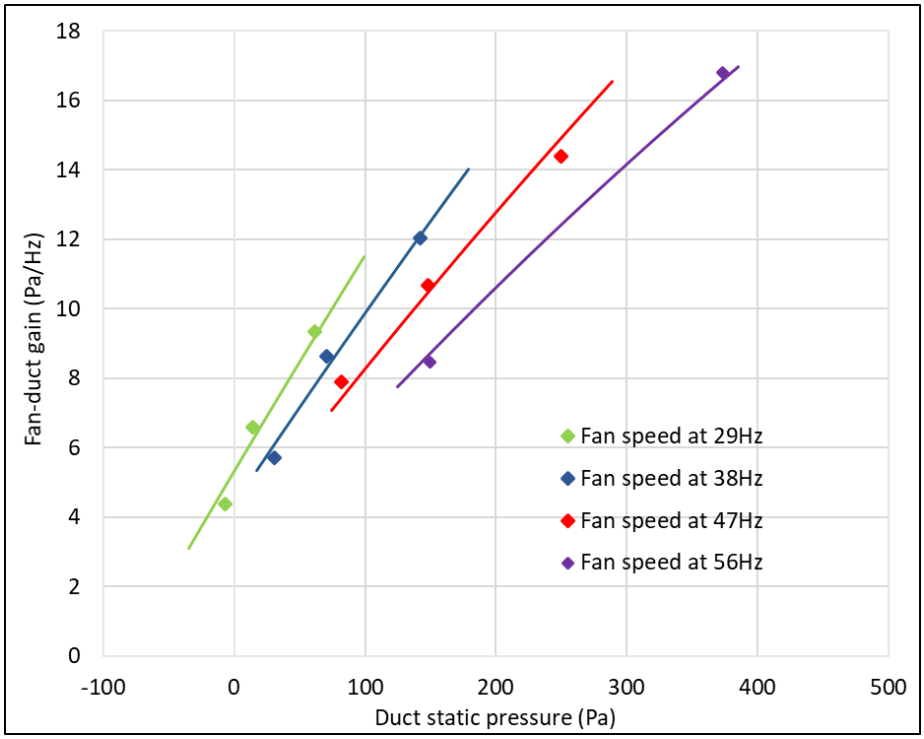

Fig. 5 Relationship between fan-duct gain and duct static pressure under various fan speeds.

Based on Fig. 5, the fan-duct gain is regressed as a function of the fan speed (N) and duct static pressure (H_{sp}), shown as Eq. (8), which has a R squared value of 0.98. For comparison, the regressed curves using Eq. (8) with the fan speed fixed at different values are also presented in Fig. 5 with the same color corresponding to the same specific fan speed.

$$K_{fd} = 0.000615N^2 - 0.1522N - 0.00001401{H_{sp}}^2 + 0.0867H_{sp} - 0.0007968N \times H_{sp} + 9.263 \quad (8)$$

In addition, the duct static pressure sensor has a time constant of 0.25 second while its gain is 1.0 Pa/Pa according to the manufacturer.

The PI controller for the closed-loop control system was tuned under the design condition with the duct static pressure setpoint at 124 Pa and the fan speed at 45Hz, where $K_P = 0.36$ %/Pa and $K_I = 0.15$ per second.

3.2 Root locus and distribution for a varying forward-path gain

Before the root distribution with variable operation conditions is discussed, the root distribution with a variable K_P in Eq. (4), is demonstrated to be equivalent to the conventional root locus. The variable K_P is achieved by adding an extra gain in the forward path, denoted as extra forward-path gain, (K_{extra}), when the system operates at the design condition with the duct static pressure setpoint of 124 Pa and the fan speed of 45Hz. Then, the closed-loop transfer function in Eq. (4) can be rewritten as Eq. (9) and the control parameters are fixed except for the extra forward-path gain (K_{extra}).

$$G(s) = \frac{K_{extra}K_P\left(1+\frac{K_I}{s}\right)\left(\frac{K_{ac}}{\tau_{ac}s+1}\right)\left(\frac{K_{pt}}{\tau_{pt}s+1}\right)}{1+K_P\left(1+\frac{K_I}{s}\right)\left(\frac{K_{ac}}{\tau_{ac}s+1}\right)\left(\frac{K_{pt}}{\tau_{pt}s+1}\right)\left(\frac{K_{sr}}{\tau_{sr}s+1}\right)} \quad (9)$$

The root locus and root distribution were sketched as the extra forward-path gain was varied to compare the root locus and the root distribution, shown in Fig. 6.

The root locus with corresponding forward-path gain in Fig. 6(a) was sketched in MATLAB using the *rlocus* command, which indicates that the control system has one pair of conjugate dominant poles. To explicitly show how the varying forward-path gain impacts the control performance, the corresponding forward-path gain can also be marked in the figure. Again, the system has the design control performance with the extra forward-path gain of 1. However, since only a limited number of gains can be added, the dominant poles for the design condition even cannot be accurately identified.

On the other hand, because the control performance may be estimated using the dominant poles and the root locus is symmetrical about the real axis, only the dominant pole with positive imaginary part needs to be presented, resulting in the root distribution with the corresponding extra forward-path gain as the third dimension, shown as Fig. 6(b), where the dominant poles can be accurately identified for a given extra forward-path gain. It should be noticed that the projection of Fig. 6(b) on the complex plane actually is Fig. 6(a) and the root locus and distribution are equivalent for a variable forward-path gain. Thus, the root distribution can replace the root locus to evaluate the system control performance. The differences between the root locus and the root distribution when only one parameter is varied are listed in Table 2.

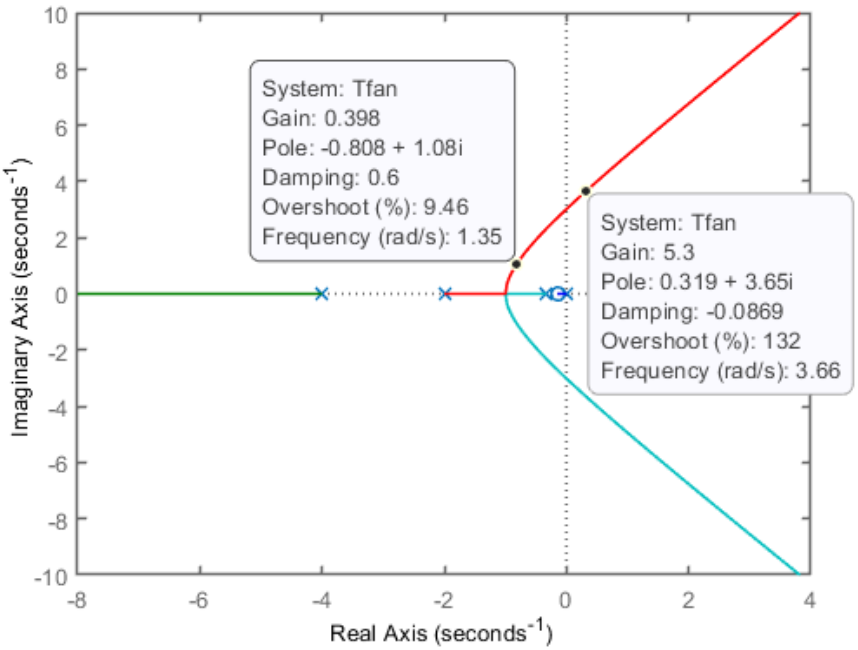

Fig. 6(a) Root locus

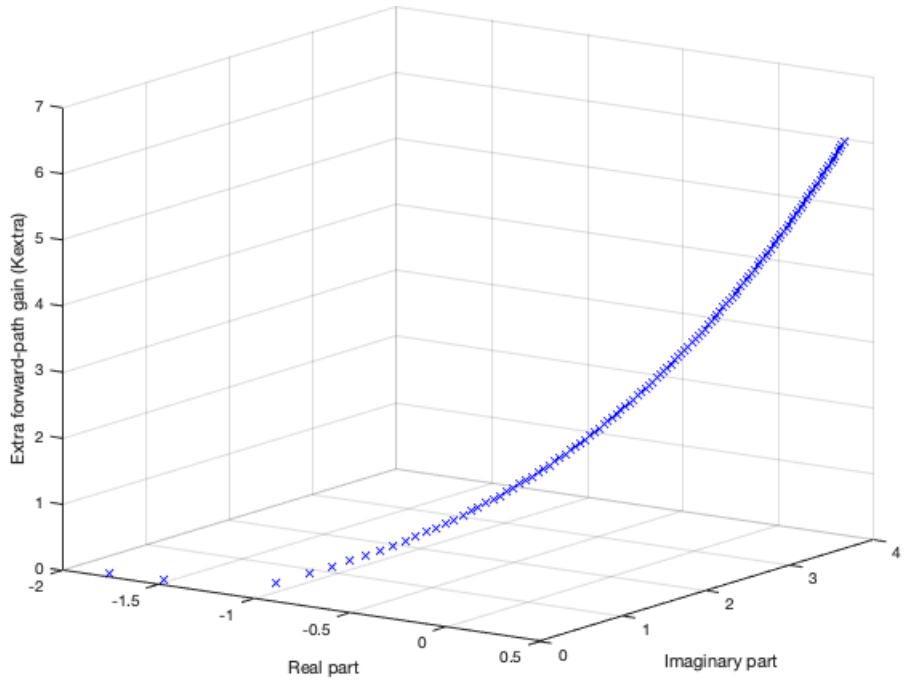

Fig. 6(b) Root distribution

Fig. 6 Root locus and root distribution for varying forward-path gain.

3.3 Root distribution for varying one operation parameter

After the demonstration of the root distribution for varying one control parameter, i.e., the variable K_P, the operation parameter-based root distribution is first demonstrated as one operation parameter is varied. To sketch the root distribution for one varying operation parameter, the remaining operation parameters and controller gains should be fixed. For example, to identify the impact of varying fan speed, the fan speed is varied from 60 Hz to 25 Hz while the duct static pressure is fixed at 124 Pa. On the other hand, to identify the impact of varying the duct static pressure, the duct static pressure is varied from 24.9 Pa to 423 Pa while the fan speed is fixed at 45 Hz.

To determine the number of operation conditions to be generated, the sensitivities of the fan-duct gain to the changes of the fan speed and duct static pressure are studied respectively. According to Eq.

(8), the sensitivities of the fan-duct gain to the changes of the fan speed change and duct static pressure are calculated as Eq. (10) and Eq. (11) respectively. The value of $\frac{\partial K_{fd}}{\partial N}$ remains smaller than 0 while the value of $\frac{\partial K_{fd}}{\partial H_{sp}}$ remains larger than 0 as the fan speed is varied from 60 Hz to 25 Hz and duct static pressure is varied from 24.9 Pa to 423 Pa, which reveals that the impacts of the fan speed and duct static pressure on the fan-duct gain are both monotonic. In this case, 80 operation conditions for varying fan speed and duct static pressure are generated in this study, which is sufficient to catch the nonlinear characteristics.

$$\frac{\partial K_{fd}}{\partial N} = 0.00123N - 0.0007968H_{sp} - 0.1522 \tag{10}$$

$$\frac{\partial K_{fd}}{\partial H_{sp}} = -0.00002802H_{sp} - 0.0007968N + 0.0867 \tag{11}$$

Fig. 7 shows the fan-duct gain and corresponding root distribution as the fan speed or duct static pressure is varied. Fig. 7(a) reveals that the fan-duct gain increases from 6.94 Pa/Hz to 13.9 Pa/Hz as the fan speed decreases from 60 Hz to 25 Hz at the duct static pressure of 124 Pa. Meanwhile, Fig. 7(c) reveals the fan-duct gain increases from 4.90 Pa/Hz to 22.5 Pa/Hz as the duct static pressure increases from 24.9 Pa to 423 Pa at the fan speed of 45Hz. The operation parameter-based root distributions are shown in Fig. 7(b) with variable fan speed and Fig. 7(d) with variable duct static pressure where only the dominant poles with positive imaginary part are displayed. Note that the closed-loop poles can still be sketched in the s-plane same as the root locus by projecting the root distribution on the s-plane. It reveals that, as the fan speed decreases from 60 Hz to 25 Hz at the duct static pressure of 124 Pa or the duct static pressure increases from 24.9 Pa to 423 Pa at the fan speed of 45 Hz, the dominant poles move towards the northeast (upper right) of the s-plane. This means that the transient response gradually

becomes more oscillatory with a longer settling time and a larger overshoot. Specifically, the dominant poles enter the RHP when the duct static pressure is more than 323 Pa at the fan speed of 45 Hz, which means that the transient response eventually becomes unstable at this operation condition.

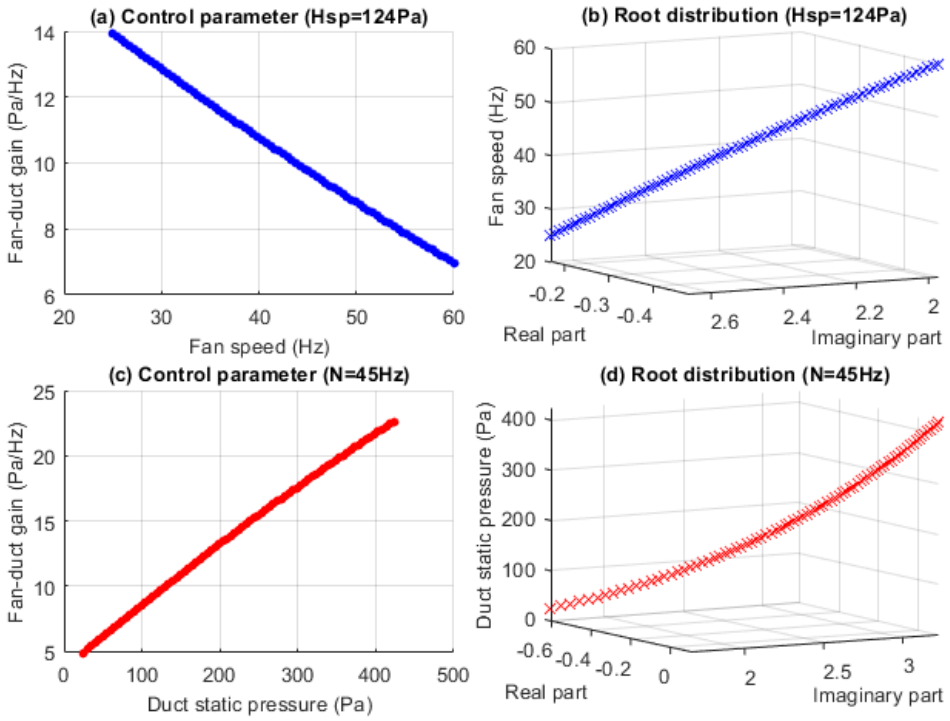

Fig. 7 Control parameters and root distributions for one varying operation parameter.

3.4 Root distribution for two varying operation parameters

The above results indicate that the fan speed control performance is sensitive to a single operation parameter variation while the remaining operation parameters are fixed. However, in practice, the operation parameters are varied simultaneously, for which it is necessary to investigate the integrated impact of the fan speed and duct static pressure and the root distribution for two varying operation parameters is critical. In this case, the conventional root locus technique cannot be applied, and the closed-loop poles cannot be directly sketched in the s-plane. Thus, the root distribution approach

becomes the only tool to evaluate the system control performance with more than one varying operation parameters.

The fan speed varies from 60 Hz to 25 Hz, and the duct static pressure varies from 24.9 Pa to 423 Pa in this investigation. Fig. 8 shows the fan-duct gain as the fan speed and duct static pressure are varied simultaneously. It reveals that the fan-duct gain has a varying range from 3.31 Pa/Hz under the operation condition where fan speed is 60 Hz and the duct static pressure is 24.9 Pa, to 31.59 Pa/Hz under the operation condition where the fan speed is 25 Hz and the duct static pressure is 423 Pa.

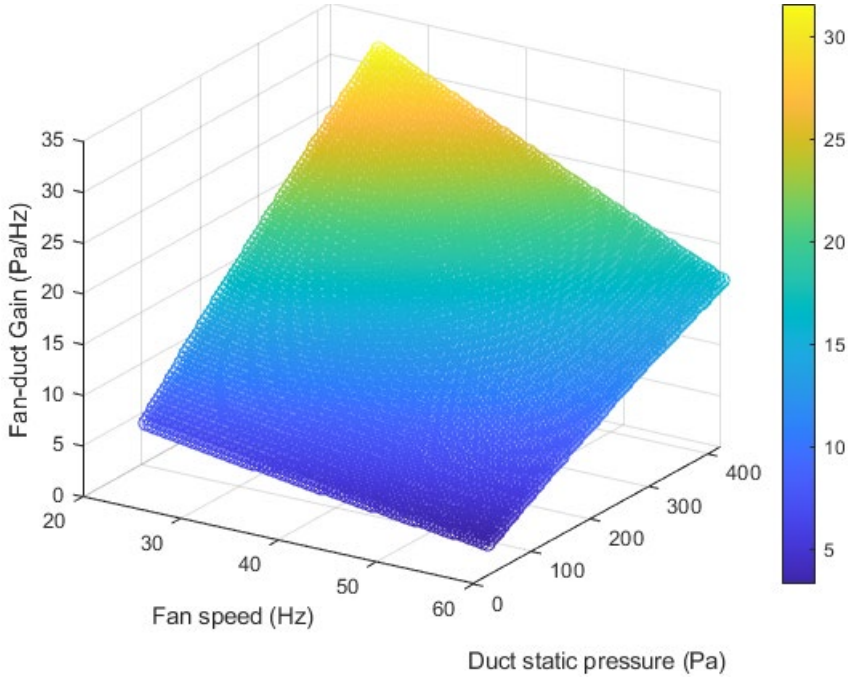

Fig. 8 Fan-duct gain varying fan speed and duct static pressure.

Correspondingly, the operation parameter-based root distribution is shown in Fig. 9 where only the dominant pole with positive imaginary part is displayed. Fig. 9(a) and Fig. 9(c) present, respectively, the real and imaginary parts of this pole as functions of the fan speed and duct static pressure, while Fig. 9(b) and Fig. 9(d) present the same information as contour lines for a clearer view. Moreover, the angle

between the pole and the negative real axis can be presented as functions of the fan speed and duct static pressure to evaluate the percent overshoot performance. Specifically, the real part of the closed pole shows a varying range from -6.839 under the operation condition where fan speed is 60 Hz and the duct static pressure is 24.9 Pa, to 0.327 under the operation condition where the fan speed is 25 Hz and the duct static pressure is 423 Pa. These contour lines exhibit a general trend: as the fan speed drops and the duct static pressure rises, the pole tends to move northeast (upper right) on the s-plane, resulting in responses that oscillate more and take longer to settle. The contour lines also define an important region—the yellow/orange/green region in Fig. 9(b) where the real part is nonnegative—in which the system is unstable. In other words, if the system is designed with constant duct static pressure setpoint, the system tends to be unstable under partial load conditions with lower fan speed.

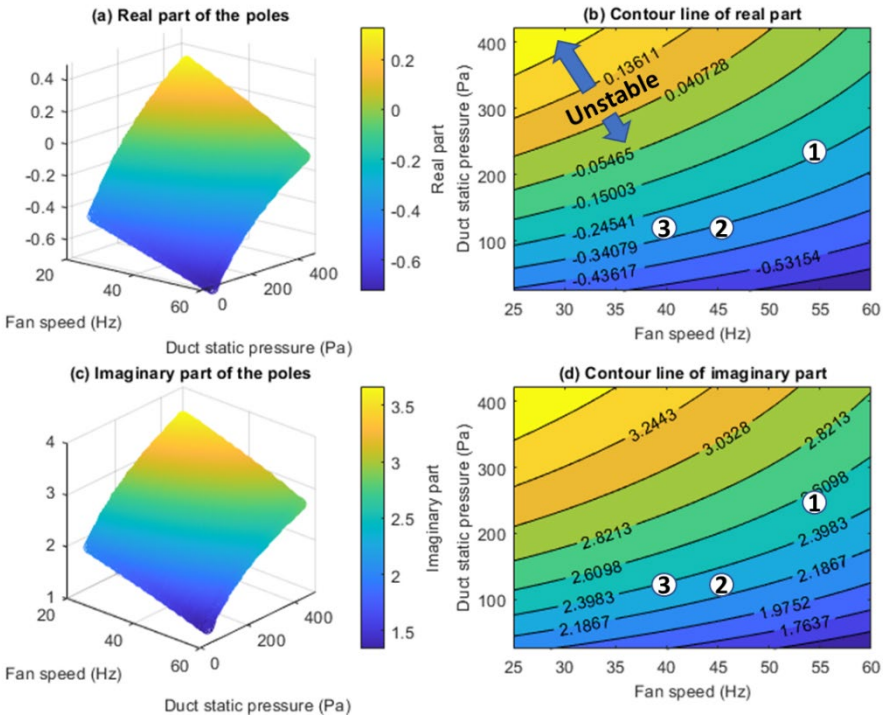

Fig. 9 Root distribution for varying fan speed and duct static pressure.

4 Validation through field tests

The findings assume that the fan speed control performance may be estimated based on the dominant poles in the root distribution. To validate this assumption and prove the reliability of the operation parameter-based root distribution, the closed-loop field tests were performed on the same fan speed control system with the fixed controller ($K_P = 0.36$ %/Pa and $K_I = 0.15$ per second) but various operation conditions.

In the first operation condition, the duct static pressure setpoint was originally set at 249 Pa. In the second operation condition, the duct static pressure was reset to 124 Pa to generate the operation conditions with a different duct static pressure while the seven terminal boxes were kept at the same flow rate setting as the first operation condition. In the third operation condition, two terminal boxes were closed by setting the terminal box maximum airflow setpoint as zero to generate different fan speeds while the duct static pressure setpoint was fixed at 124 Pa.

Three operation conditions are marked by Points 1 to 3 in the contour line of real part (b) and imaginary part (d) in Fig. 9. It can be observed that Point 1 has the smallest (negative) real part and largest imaginary part, while Point 2 has the largest (negative) real part and smallest imaginary part. Thus, by geometry, the dominant poles at Point 1 have the largest angle (θ), followed by those at Points 3 and 2. Therefore, by following Eqs. (5), it is expected that the time response with reference input at Point 2 should have the smallest settling time, largest peak time, and smallest overshoot, the time response at Point 1 should have the opposite behavior, and the time response at Point 3 should be

somewhere in between. In other words, the system with the operation condition at Point 1 is expected to have the most aggressive response, followed by those at Points 3 and 2.

Fig. 10 shows the system transient response of the measured fan speed (blue line) and duct static pressure (green line) under the three operation conditions marked by the same points as in Fig. 9. O'Neill, Li et al (O'Neill, Li, and Williams 2017) conducted a comprehensive review of control loop performance assessments. In their study, 14 indices are considered suitable for implementation in HVAC control loop performance assessment. In our case, because the system response is too fast to accurately catch the dynamic response specifications using the recorded data with a sampling time of 1 second, the control performance impacted by the noise and system oscillation at the steady-state conditions is evaluated instead, which can also reflect the aggressiveness and stability of the response. Therefore, the control performance is evaluated by using three numerical indices, including the oscillation range of the fan speed and duct static pressure, and the root mean squared error (RMSE) of the duct static pressure.

The oscillation range is defined as the difference between the average maximum value and the average minimum value of the fan speed or duct static pressure at each operation condition; the RMSE of the duct static pressure is calculated using Eq. (12). Since the fan speed varies as the operation condition is changed, the RMSE of the fan speed is not evaluated.

$$RMSE = \sqrt{\frac{\sum_{j=1}^{n}(H_{spj,measured} - H_{spj,setpoint})^2}{n}} \quad (12)$$

where $H_{spj,measured}$ and $H_{spj,setpoint}$ refer to the measured value and the setpoint of the duct static pressure at the jth sample respectively; n is the total number of the measured samples. Table 4 lists the

oscillation range of the fan speed and duct static pressure as well as the RMSE of the duct static pressure under the three test conditions.

Table 4: Oscillation range and RMSE under the three test conditions.

Test condition	Real Part of the dominant poles	Fan speed oscillation range (Hz)	Duct static pressure oscillation range (Pa)	RMSE of duct static pressure (Pa)
Condition 1	-0.2237	2.0	28.6	11.9
Condition 2	-0.3402	0.44	6.10	2.44
Condition 3	-0.2789	0.83	12.2	5.05

It is obvious that operation condition 1 has the smallest negative real part of the dominant poles. It has the most aggressive response with the largest fan speed oscillation range of 2.0 Hz, the duct static pressure oscillation range of 28.6 Pa, and the RMSE of duct static pressure of 11.9 Pa, operation condition 2 has the largest negative real part of the dominant poles. It has the most stable response with the smallest fan speed oscillation range of 0.44 Hz, the duct static pressure oscillation range of 6.10 Pa, and RMSE of duct static pressure of 2.44 Pa, and operation condition 3 has a negative real part and control performance in between. The system response from the tests in Fig. 10 match with the expectations from Fig. 9. This result validates that the fan speed control performance can indeed be estimated via the dominant poles in the root distribution. More broadly, the result illustrates the potential power of operation parameter-based root distribution in predicting control system performance without time-domain simulation.

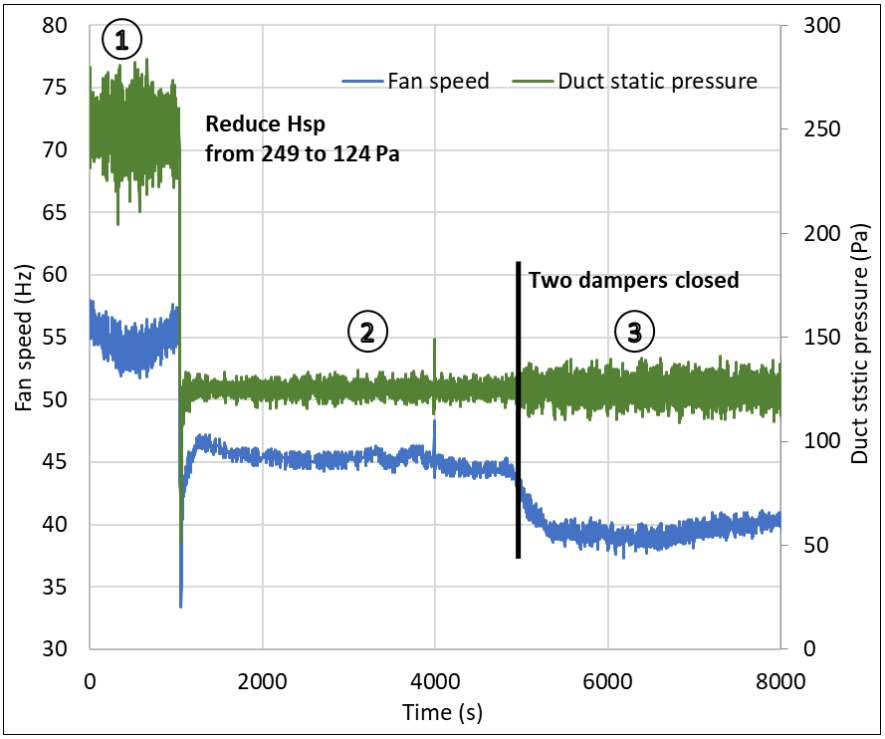

Fig. 10 System transient response under the three operation conditions.

It has to be noted that, the root distribution in Fig. 9 is related to the controller design. For example, if the controller has a larger P gain, all the contour lines of the real part will move downward, and the unstable region will become larger. As a result, the control system may become unstable under operation condition 1 while remain stable under operation condition 2.

5 Conclusion and future work

The operation parameter-based root distribution developed in this paper can predict the performance of nonlinear control systems without time-domain simulation at all possible operation conditions and identify the impact of varying one or multiple operation parameters, which can provide both qualitative and quantitative information for the design of more effective control strategies at AHUs, such as the design of gain scheduling controller and the evaluation of its effectiveness.

The performance of a fan speed control system was evaluated as an example to illustrate the proposed approach. With its fixed PI controller tuned under a design condition, the operation parameter-based root distribution indicated that the supply fan would oscillate or even destabilize with low fan speed and high duct static pressure, which was validated through the field tests.

The application of the operation parameter-based root distribution can be extended to any control system at AHUs with more than two variable operation parameters in predicting its transient response and stability. In this case, the component gains and time constants are to be expressed as the function of all the variable operation parameters. In the future, this approach will be applied to evaluate the control performance of the cooling coil valve control systems, whose component gains and time constants are dependent on three operation parameters, including the chilled-water loop pressure differential, supply airflow rate, and mixing air temperature, if the chilled-water supply temperature is constant. To sketch the root distribution, the component gains and time constants are to be derived as the function of the three operation parameters. To visualize it, the three operation parameters can be the three dimensions as X, Y and Z axes while the real part and imaginary part can be presented in different colors respectively.

Acknowledgement

This material is based upon work supported by the U.S. Department of Energy's Office of Energy Efficiency and Renewable Energy (EERE) under the Building Technologies Office, Award Number DE-EE0008683.

Disclaimer

The views expressed herein do not necessarily represent the views of the U.S. Department of Energy or the United States Government.

Nomenclature

CO = VFD frequency command

H = pressure (Pa)

k = number of closed poles

K = gain (%/Pa, Hz/%, Pa/Hz)

G, H = transfer function

l = order of the controller

m = number of operation parameters

n = number of components

N = fan speed (Hz)

Po = pole

t = time (s)

Num = number of operation conditions

σ_d = negative of the real part of the complex pole

θ = angle

τ = time constant (s)

μ = operation parameter

ω_d = imaginary part of the complex pole

Subscripts and superscripts:

ac = actuator

ct = component

C = controller

fd = fan-duct

sd = studied

sp = static pressure

I = integral

i, j = ith sample, jth sample

n = total number of samples

pt = plant

P = proportional

sr = sensor

Vm = VFD-motor

Reference

Adebayo, Isaiah, David Aborisade, and Ogunkeyede Yinka. 2020. 'A Comparative Analysis of SIMC-PID with Other Conventional Techniques for Automobile Vehicle Air Conditioning System Control', *Journal of Scientific Research and Reports*: 27-38.

Al-Khayat, Rasha Hayder, Ali Wadi Abbas Al-Fatlawi, Maher AR Sadiq Al-Baghdadi, and Muhannad Al-Waily. 2022. 'Water hammer phenomenon in pumping stations: A stability investigation based on root locus', *Open Engineering*, 12: 254-62.

Almabrok, Abdoalnasir, Mihalis Psarakis, and Anastasios Dounis. 2018. 'Fast tuning of the PID controller in an HVAC system using the big bang–big crunch algorithm and FPGA technology', *Algorithms*, 11: 146.

Barwig, Floyd E, John M House, Curtis J Klaassen, Morteza M Ardehali, and Theodore F Smith. 2002. "The national building controls information program." In *Proc. ACEEE summer study on energy efficiency in buildings*.

Chintala, Rohit, Christopher Price, Shuangshuang Liang, and Bvan P Rasmussen. 2015. 'Identification and Elimination of Hunting Behavior in HVAC Systems', *ASHRAE Transactions*, 121.

Dincel, Emre, and Mehmet Turan Söylemez. 2016. "Limitations on dominant pole pair selection with continuous PI and PID controllers." In *Proc. IEEE International Conference on Control, Decision and Information Technologies (CoDIT)*, 741-45.

Evans, Walter R. 1948. 'Graphical analysis of control systems', *Transactions of the American Institute of Electrical Engineers*, 67: 547-51.

Flower, J.O., and C.G. Hodge. 2004. 'Stability and transient-behavioural assessment of power-electronics-based dc-distribution systems: Part 1: The root-locus technique', *Journal of Marine Engineering & Technology*, 3: 13-21.

Lachi, M, N El Wakil, and J Padet. 1997. 'The time constant of double pipe and one pass shell-and-tube heat exchangers in the case of varying fluid flow rates', *International Journal of Heat and Mass Transfer*, 40: 2067-79.

Mei, L, and GJ Levermore. 2002. 'Simulation and validation of a VAV system with an ANN fan model and a non-linear VAV box model', *Building and Environment*, 37: 277-84.

Moradi, Hamed, Majid Saffar-Avval, and Firooz Bakhtiari-Nejad. 2011. 'Nonlinear multivariable control and performance analysis of an air-handling unit', *Energy and Buildings*, 43: 805-13.

Mulligan, James Henry. 1949. 'The effect of pole and zero locations on the transient response of linear dynamic systems', *Proceedings of the IRE*, 37: 516-29.

Nassif, Nabil. 2010. 'Performance analysis of supply and return fans for HVAC systems under different operating strategies of economizer dampers', *Energy and Buildings*, 42: 1026-37.

Nise, Norman S. 2019. *Control Systems Engineering, 8th Edition* (Wiley: Hoboken, NJ, USA).

O'Neill, Zheng, Yanfei Li, and Keith Williams. 2017. 'HVAC control loop performance assessment: A critical review (1587-RP)', *Science and Technology for the Built Environment*, 23: 619-36.

Pérez Lombard, Luis, José Ortiz, and Christine Pout. 2008. 'A review on buildings energy consumption information', *Energy and Buildings*, 40: 394-98.

Price, Christopher, Shuangshuang Liang, and Bryan Rasmussen. 2015. 'HVAC nonlinearity compensation using cascaded control architectures', *ASHRAE Transactions*, 121: 217.

Price, Christopher Robin. 2018. 'Cascaded Control for Improved Building HVAC Performance', Texas A & M University.

Singhal, Ashish, and Timothy I Salsbury. 2007. 'Characterization and Cancellation of Static Nonlinearity in HVAC Systems', *ASHRAE Transactions*, 113.

Underwood, Chris P. 2002. *HVAC Control Systems: Modelling, Analysis and Design* (Routledge).

Wang, Gang, and Zhitao Han. 2019. 'Investigation of the accuracy of VFD analog output data and the energy performance of different voltage controls in a VFD-motor-belt-fan system', *Energy and Buildings*, 194: 260-72.

Wang, Gang, Li Song, and Kaustubh Phalak. 2015. 'Investigation of the fan energy and control performance of different damper control strategies in air handling units', *ASHRAE Transactions*, 121: 110-22.

Wang, Qingguo, Zhiping Zhang, Karl Johan Astrom, Yu Zhang, and Yong Zhang. 2009. 'Guaranteed dominant pole placement with PID controllers', *Journal of Process Control*, 19: 349-52.